Using the Generalized Inverted Pendulum to generate less energy-consuming trajectories for humanoid walking

Sahab Omran, Sophie Sakka, Yannick Aoustin

Keywords: Inverted pendulum, pivot point, walking robots, energy consumption, joint torques

Using the Generalized Inverted Pendulum to generate less energy-consuming trajectories for humanoid walking

Sahab Omran[*], **Sophie Sakka**[†], **Yannick Aoustin**[‡]

Abstract

This paper proposes an analysis of the effect of vertical position of the pivot point of the inverted pendulum during humanoid walking. We introduce a new feature of the inverted pendulum by taking a pivot point under the ground level allowing a natural trajectory for the center of pressure (CoP), like in human walking. The influence of the vertical position of the pivot point on energy consumption is analyzed here. The evaluation of a 3D Walking gait is based on the energy consumption. A sthenic criterion is used to depict this evaluation. A consequent reduction of joint torques is shown with a pivot point under the ground.

1 Introduction

The linear inverted pendulum (LIP) was proposed by Kajita *et al.* to generate humanoid walking trajectories [Kaj01, Kaj91]. This model was widely applied to various bipedal robots like HRP-2 [Ais98], Asimo [Hon96], and UT-Theta [UT01]. The main advantage of this approach is the simplicity of the dynamics and the analytical solution.

The inverted pendulum has also been used for the modeling of human walking. The first pendulum model of human walking considers that the zero moment point (ZMP) within the simple support is a fixed point in the foot center [Zij97]. However, biomechanical research shows that the human ZMP moves forward, towards the big toe, during the single support [Har09]. To embed this feature of ZMP in the pendulum model of human walking, Hayot *et al.* proposed a pendulum with a pivot point that moves during the single support [Hay13]. This pendulum allows to reproduce the natural foot roll of human.

Rolling of feet in human walking consists in moving the supporting area during the support phase of each foot, from the heel, through the middle of foot to the toe. While human is rolling its feet, the ZMP follows the supporting area in order to keep the equilibrium.

However, in the model of Hayot *et al.* the advancement of the ZMP in the single support requires a strict definition [Hay13]. Later, the Generalized Inverted Pendulum model (GIP) [Sak10] was suggested by Sakka *et al.* for human walking modeling. The GIP has a pivot point under the ground level in opposition to all other inverted pendulum models (for robot control or human motion) with a pivot point at ground level. It describes human normal walking from the external forces point of view, taking into account the mechanism of foot.

The contribution of this paper is to extend the GIP [Sak10] to generate a human inspired walking pattern of humanoid robots. We analyze the influence of the pivot point depth on the geometric behavior of the pendulum. We present the adopted constraints on the position of the pivot point, depending on the size of the robot feet. We study also the influence of the pivot point depth on joint torques. Finally, we analyze the energy consumption of Romeo humanoid robot during walking using two criteria: sthenic criterion and energy criterion. The influence of the step length was also introduced.

[*]LUNAM, IRCCyN, CNRS, Ecole Centrale de Nantes, University of Nantes. 1, rue de la Noë BP 92101. 44321 Nantes, France. E-mail: sahab.omran@irccyn.ec-nantes.fr

[†]IRCCyN, University of Poitiers, France. E-mail: sophie.sakka@irccyn.ec-nantes.fr

[‡]LUNAM, IRCCyN, CNRS, Ecole Centrale de Nantes, University of Nantes. 1, rue de la Noë BP 92101. 44321 Nantes, France. E-mail: yannick.aoustin@irccyn.ec-nantes.fr

Acknowledgement : This work is supported by Région des Pays de la Loire, Project *LMA* and Gérontopôle Autonomie Longévité des Pays de la Loire.

This paper is organized as follows: In section 2, we show that the dynamics equations system does not change if the pivot point is located under the ground or at ground level. The calculations of joint angles and joint torques are given in section 3. The evaluation criteria are presented in section 4. Simulation setting and the Romeo robot description are given in section 5. Results demonstrating the efficiency of the method from the joint torques viewpoint are displayed in section 6. Finally, we conclude and we show our perspectives in section 7.

2 Dynamics equation for an inverted pendulum with a pivot point under the ground

In this section, we will study the dynamics of the inverted pendulum in the general case: The CoM is not constrained to maintain a constant height during the movement and whose pivot point is located under the ground. Fig. 1 illustrates the inverted pendulum in the sagittal plane, where the mass M moves under the force f and the gravity g. The mass is connected to the ground with a massless rod. The pivot point of the

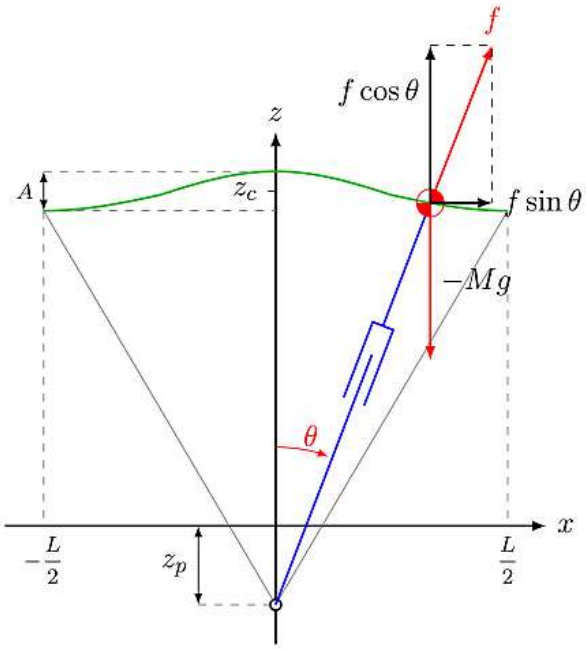

Figure 1: Generalized inverted pendulum in the sagittal plane.

pendulum is a virtual revolute joint located under the ground, z_p is its vertical component. θ is the angle between the rod and the vertical axis. The global coordinates system is defined by the forward $\mathbf{x}$-axis, the up-ward vertical $\mathbf{z}$ -axis and the lateral axis $\mathbf{y} = \mathbf{z} \times \mathbf{x}$.
The force f and the gravity create an acceleration of the CoM $[\ddot{x}\ \ddot{y}\ \ddot{z}]^\top$.

$$\text{Along the vertical } \mathbf{z}\text{-axis} \ : \qquad f\cos\theta - Mg = M\ddot{z} \tag{1}$$

$$\text{Along the forward } \mathbf{x}\text{-axis} \ : \qquad f\ \sin\theta = M\ \ddot{x} \tag{2}$$

By substituting (1) in (2), we obtain

$$(g+\ddot{z})\ \frac{\sin\theta}{\cos\theta}\ =\ \ddot{x} \tag{3}$$

$$\frac{\sin\theta}{\cos\theta} = \tan\theta\ = \frac{x}{z-z_p} \tag{4}$$

The minus sign of z_p is justified by the fact that $z_p \leq 0$.

$$x\ =\ \frac{z-z_p}{g+\ddot{z}}\ \ddot{x} \tag{5}$$

In a similar manner, we obtain the motion equation in the frontal plane.

$$y = \frac{z - z_p}{g + \ddot{z}}\, \ddot{y} \tag{6}$$

The motion of the CoM is characterized by the second order differential equations (5) and (6). These equations are very similar to those in the case where the pivot point is located at ground level. The only difference is that the term z is replaced by $z - z_p$. In some previous works devoted to walking, the term z_p was used to express the vertical component of origin of the frame attached to the foot with respect to the global coordinate system and the pivot point was always in the foot. But now, z_p expresses the vertical distance between the pivot point and the ground. The differential equations 5 and 6 can be solved analytically when $z = const$. When $z \neq const$, these two equations are solved numerically.

3 Modeling

Let us consider a humanoid robot composed of n_{act} actuators to control its body movements in 3D. Let $\mathbf{q}$ and $\mathbf{X}$ denote the system generalized and operational coordinates vectors, respectively. We introduce the following notations:

$\mathbf{X}$	(6×1)	Absolute position and orientation of the waist ;
$\mathbf{X}_{f_i}$	(6×1)	Absolute position and orientation of foot i $(i = 1, 2)$;
$\mathbf{q}_{leg_i}$	$(n_{leg} \times 1)$	Actuated joints of leg$_i$ (ankle, knee and hip joints);
$\mathbf{q}$	$(n \times 1)$	Vector grouping the controlled variables $(n = n_{act} + 6)$.

The vector $\mathbf{q}$ contains the joint variables and the 3D position and orientation of the frame R_0 fixed in the left foot. The reference frame is defined such that $\mathbf{x}_0$ denotes the horizontal advancement direction, $\mathbf{z}_0$ is the vertical bottom-up direction, and $\mathbf{y}_0 = \mathbf{z}_0 \times \mathbf{x}_0$ is the lateral direction.

3.1 Walking cycle – Assumptions

The walking cycle is defined by two successive steps (right and left legs). One step is composed of a single support phase (SS) on the stance leg, delimited by swinging foot takeoff and swinging foot strike, and a double support phase (DS) where the body weight is distributed on both legs, delimited by swinging foot strike and other foot takeoff. In what follows, the following assumptions will be considered for the complete motion:

A1 There is no rotation of the swing foot and the pelvis of the biped with respect to the roll, pitch, and yaw axes.

A2 The stance foot has a flat contact on the ground;

A3 Feet velocity and acceleration are equal to zero at foot strike. Thus no impact is considered.

A4 The CoM and the waist segment have the same linear velocity and acceleration profiles;

As humanoid systems are highly redundant, these assumptions allow setting the control schemes while reducing the redundancy order by setting arbitrarily several parameters. The motion of the swinging foot is defined as a polynomial function, where the polynomial coefficients were determined using initial and final positions, velocities, and accelerations.

3.2 Kinematics

For given desired Cartesian trajectories of the waist $\mathbf{X}$ and the feet $\mathbf{X}_{f_i}$ $(i = 1, 2)$, the inverse kinematics model leads to the values of the desired joint variables as follows

$$\begin{bmatrix} \mathbf{V}_{f_i} \\ \omega_{f_i} \end{bmatrix} = \begin{bmatrix} \mathbf{I}_{3\times3} & -\hat{\mathbf{L}} \\ \mathbf{0}_{3\times3} & \mathbf{I}_{3\times3} \end{bmatrix} \begin{bmatrix} \mathbf{V} \\ \omega \end{bmatrix} + \mathbf{J}_{leg_i} \dot{\mathbf{q}}_{leg_i} \qquad (i = 1, 2) \tag{7}$$

where $\dot{\mathbf{X}}_{f_i} = [\mathbf{V}_{f_i}^\top \ \omega_{f_i}^\top]^\top$, $\dot{\mathbf{X}} = [\mathbf{V}^\top \ \omega^\top]^\top$, $\mathbf{J}_{leg_i}$ $(i = 1, 2)$ denotes the $6 \times n_{leg}$ Jacobian matrix associated to the i-th leg, $\mathbf{L}$ is the position vector between the waist and foot f_i and $\hat{\mathbf{L}}$ is the skewsymetric matrix of $\mathbf{L}$. Due to assumption **A1**, $\omega = \omega_{f_i} = 0$, thus (7) becomes

$$\dot{\mathbf{q}}_{leg_i} = \mathbf{J}_{leg_i}^{-1} \begin{bmatrix} \dot{\mathbf{X}}_{f_i} - \dot{\mathbf{X}} \\ \mathbf{0}_{3\times1} \end{bmatrix} \qquad (i = 1, 2) \tag{8}$$

The desired $n \times 1$ controlled velocities vector $\dot{\mathbf{q}}$ can be rebuilt as follows.

$$\dot{\mathbf{q}} = \left[\dot{\mathbf{q}}_{leg_1}\ \dot{\mathbf{q}}_{leg_2}\ \dot{\mathbf{q}}_{free}\ \dot{\mathbf{X}}\right]^\top \tag{9}$$

where $\dot{\mathbf{q}}_{free}$ denotes joint velocities of trunk and arms which can be set freely.

The rank of the Jacobian matrix of each leg was verified at each sampling period of motion to ensure that there is no singularity.

3.3 Dynamics

The dynamics of the system may be described by the three following equations.

$$\begin{cases} \mathbf{D}\ddot{\mathbf{q}} + \mathbf{C}\dot{\mathbf{q}} + \mathbf{G} = \mathbf{B}\boldsymbol{\Gamma} + \mathbf{J}_1^\top \mathbf{R}_1 & \text{if in single support on leg}_1 \\ \mathbf{D}\ddot{\mathbf{q}} + \mathbf{C}\dot{\mathbf{q}} + \mathbf{G} = \mathbf{B}\boldsymbol{\Gamma} + \mathbf{J}_2^\top \mathbf{R}_2 & \text{if in single support on leg}_2 \\ \mathbf{D}\ddot{\mathbf{q}} + \mathbf{C}\dot{\mathbf{q}} + \mathbf{G} = \mathbf{B}\boldsymbol{\Gamma} + \mathbf{J}_1^\top \mathbf{R}_1 + \mathbf{J}_2^\top \mathbf{R}_2 & \text{if in double support} \end{cases} \tag{10}$$

The matrices $\mathbf{D}(\mathbf{q})$, $\mathbf{C}(\mathbf{q},\ \dot{\mathbf{q}})$, and $\mathbf{G}(\mathbf{q})$ describe respectively the inertia, Coriolis and gravity forces acting on the system. $\boldsymbol{\Gamma}$ is the vector of the actuator torques $\boldsymbol{\Gamma}_i$, $i = 1, \cdots, nact$. Matrix $\mathbf{B}$ is the actuation matrix; it expresses the contribution of each joint torque in the virtual work δw:

$$\delta w = \boldsymbol{\Gamma}_1 \delta q_1 + \boldsymbol{\Gamma}_2 \delta q_2 + \ldots + \boldsymbol{\Gamma}_{n_{act}} \delta q_{n_{act}} = \delta \mathbf{q}^\top \mathbf{B}\boldsymbol{\Gamma}$$

where $\boldsymbol{\Gamma} = \left[\boldsymbol{\Gamma}_1\ \boldsymbol{\Gamma}_2\ \ldots\ \boldsymbol{\Gamma}_{n_{act}}\right]^\top$ and $\mathbf{B} = \left[\mathbf{0}_{n_{act}\times 6}\ \ \mathbf{I}_{n_{act}}\right]^\top$. The vectors $\mathbf{R}_1$ and $\mathbf{R}_2$ are the ground reaction forces exerted on foot$_1$ and foot$_2$ respectively.

$$\mathbf{R}_1 = \left[R_{1x}\ R_{1y}\ R_{1z}\ M_{1x}\ M_{1y}\ M_{1z}\right]^\top \qquad \mathbf{R}_2 = \left[R_{2x}\ R_{2y}\ R_{2z}\ M_{2x}\ M_{2y}\ M_{2z}\right]^\top$$

In single support, there are n unknown variables which are the components of $(\boldsymbol{\Gamma}, \mathbf{R}_1)$ or $(\boldsymbol{\Gamma}, \mathbf{R}_2)$ depending on which foot is in contact with the ground. So, the n independent equations in the two first lines of (10) are sufficient for solving. On the other hand, in double support there are $n+6$ unknown variables in $(\boldsymbol{\Gamma}, \mathbf{R}_1, \mathbf{R}_2)$ and only n equations available. In order to solve the problem in double support, six variables should be chosen and set to completely describe the system dynamics. The variables we choose are the six components of the ground reaction forces exerted on the foot that was supporting before the considered double support. Similarly to Omran *et al.* [Omr14], these components are defined as third-order polynomial functions of time ensuring the continuity of the ground reaction forces with the two single support phases around the considered double support.

In our simulation, we have tested many polynomial functions for the components of the ground reaction forces with different polynomial orders and we obtained almost the same behavior for the sthenic and the energy criteria.

4 Energy consumption

Many criteria exist to evaluate energy consumption of a mechanical system, however to our best knowledge there is no ideal criterion [Che08]. In this approach, we chose two criteria:

Sthenic criterion is defined by the integral of the quadratic actuators torques per unit of distance, as shown in (11). Its physical meaning is to be an image of the Joule effects if the actuators are DC motors. Furthermore, the torque amplitudes are decreased with the minimization of this criterion [Che01]. Then if we design an optimal walking gait with this criterion we can limit the weight of the needed motors.

$$C_\Gamma = \frac{1}{d} \int_{t_0}^{t_f} \boldsymbol{\Gamma}^\top \boldsymbol{\Gamma} \mathrm{d}t \tag{11}$$

where t_0 and t_f denote the beginning and ending instants of the total observed motion, d is the traveled distance. The sthenic criterion is a quantity proportional to the energy consumed by actuators per unit of distance, while the quadratic torque deals with the squared norm of motor torques: $E_0(t) = \boldsymbol{\Gamma}^\top \boldsymbol{\Gamma}$.

Energy criterion relates to the work done by the motors during motion. Soechting *et al.* [Soe95] proposed the minimization of work to predict the posture of the arm while moving the hand from one point to another. They have shown that the movements performed by the arms are conducted so as to minimize

the energy expended to move the hand from the initial position to the final position. The cost function is given as follows

$$W = \int_{t_0}^{t_f} \mathbf{\Gamma}\, \Omega \, \mathrm{d}t \tag{12}$$

Where $\Omega = \mathrm{d}\theta/\mathrm{d}t$ is joint velocities vector.

The minimization of work done by the joints is widely used in optimal trajectory generation [Ber08, Che08, Haq12].

5 Simulation settings

For the validation of method, we use the model of the 33 degrees-of-freedom (DOF) humanoid robot Romeo[Ald12, Ack12]. The robot total weight is 40.53 kg and its height is 1.43 m. Romeo DOF are distributed as follows: 6 per leg, 1 for each toe, 7 per arm, 1 for the trunk, 2 for the neck and 2 for the head. As we focus on the locomotion, only the 12 DOF of the legs were controlled in motion and the other DOF were set to zero. The kinematic chain of the lower body of Romeo is shown in Fig. 2.

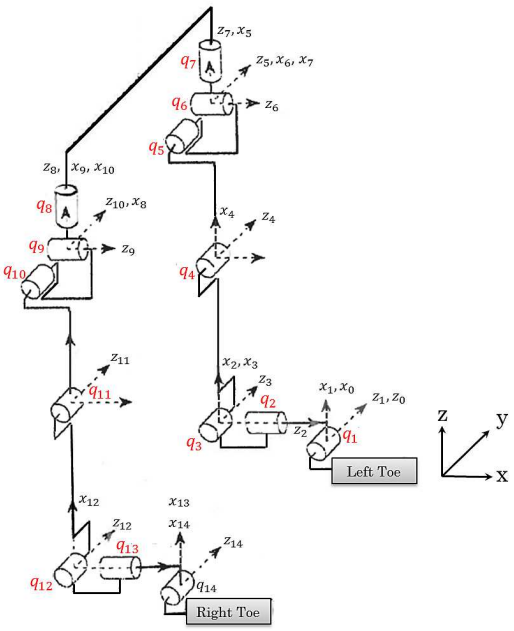

Figure 2: Lower body of humanoid robot Romeo.

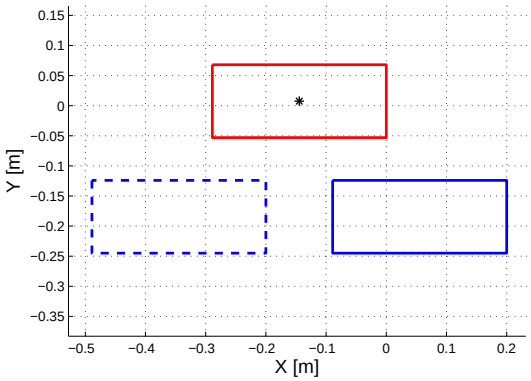

Figure 3: Feet placement for motion planing. The projection of the pivot point in the horizontal plane is represented by the black asterisk.

To show the effect of the vertical position of pivot point, the robot performs one step forward on a flat surface. The step length is set to 0.4 m, the step width is set to 0.192 m and the step duration is 0.5 sec. The height of the CoM is constant $z_c = 0.64$ m. The horizontal position of the pivot point is set in the left foot center, so the robot takes one step forward with its right foot, as shown in Fig. 3. This motion is done many times, with different depth of the pivot point z_p taken in the range $[0, -1]$ m. After calculating the CoM trajectory in the horizontal plane, we obtain joint angles using the inverse kinematic model, then we calculate the joint torques using the dynamic model. In the end, we calculate the sthenic criterion for each trajectory.

6 Results

The resulting trajectories for each z_p are compared in terms of dynamic balance, joint torques and energy consumption.

6.1 Horizontal trajectory of CoM

The motion described in Sec. 5 is realized by the robot Romeo in five cases corresponding to five values of z_p: $[0, -0.25, -0.5, -0.75, -1]$ m. Fig. 4 shows the five resulting CoM trajectories in $\mathbf{x}$ and $\mathbf{y}$ directions

as a function of time. We note that the **x** component of the CoM comes closer to a straight line when $|z_p|$ increases. On the other hand, the oscillation amplitude of the **y** component decreases when the pivot point goes farther under the ground.

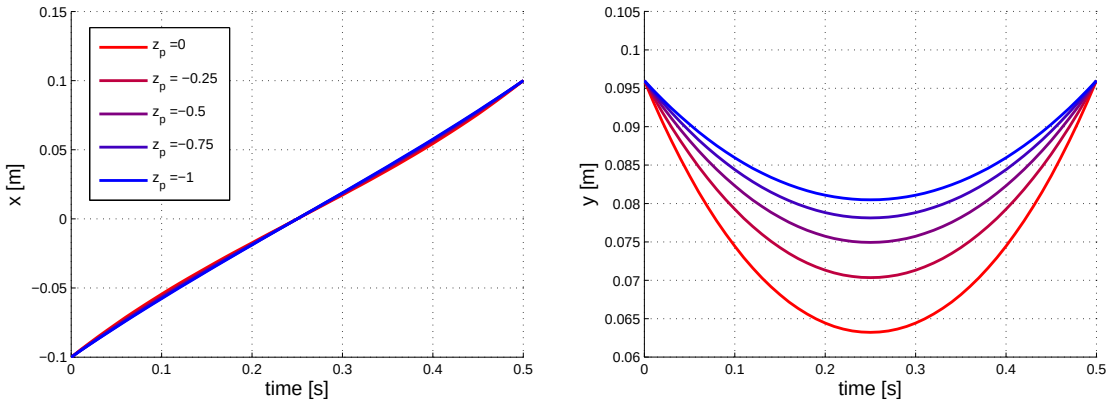

a) Forward axis b) Lateral axis

Figure 4: Horizontal trajectory of CoM as a function of time for five values of z_p

6.2 Trajectory of CoP

Fig. 5 represents two inverted pendulums. The first one with a pivot point at ground level ($z_p = 0$), its motion in the sagittal and frontal planes is represented in Fig. 5(a) and Fig. 5(c) respectively. The second one with a pivot point under ground level ($z_p = -1\ m$), its motion in the sagittal and frontal planes is represented in Fig. 5(b) and Fig. 5(d) respectively.

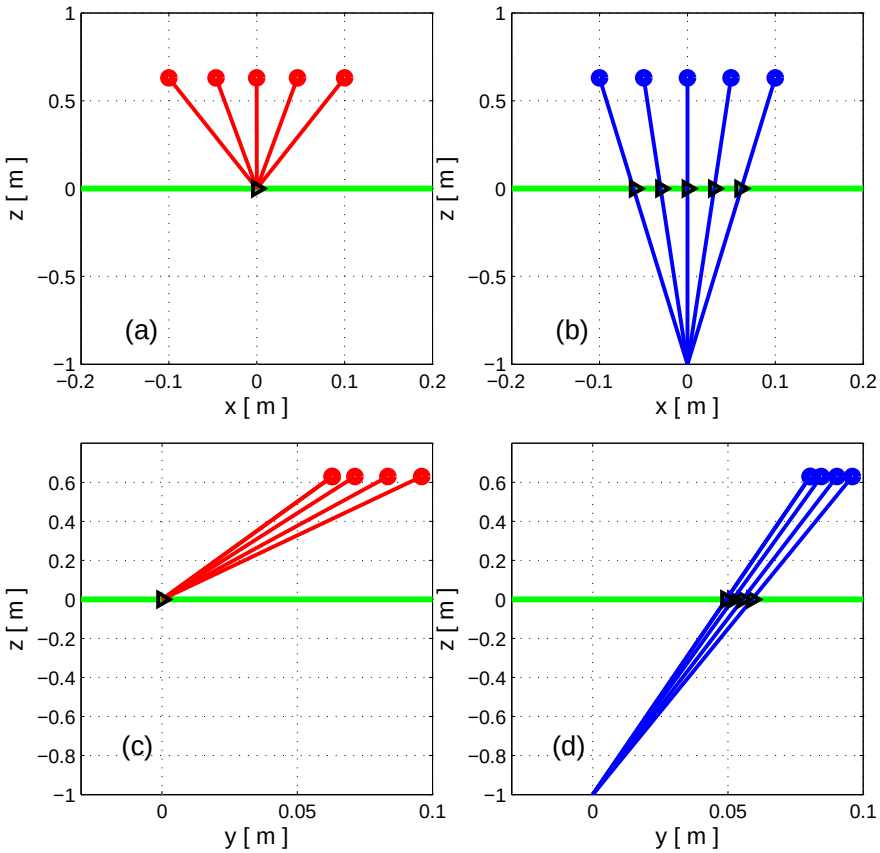

Figure 5: The inverted pendulum motion in sagittal and frontal planes in two cases: $z_p = 0$ and $z_p = -1\ m$

In Fig. 5, the CoM is represented by circles and the CoP is represented by triangle symbols. The ground level ($z = 0$) is represented by a green line. We notice that the CoP coincides with the pivot point when $z_p = 0$. In this case, the CoP is a fixed point. But when the pivot point is under the ground level, the CoP moves in x and y directions as we can see in Fig. 5(b) and Fig. 5(d) respectively. For this reason, we must verify that the distances traveled by the CoP in **x** and **y** directions are smaller than the robot foot dimensions before applying the trajectory to a humanoid robot.

To describe the relation between the CoP trajectory and the depth of the pivot point, we consider three inverted pendulums having the same parameters of step length L, step width L_w, and the CoM height z_c. The pivot point depth for these pendulums are $z_{p1} = 0$, z_{p2} and z_{p3} such as $0 < |z_{p2}| < |z_{p3}|$. These three pendulums are illustrated in Fig. 6 in the sagittal and frontal planes. The foot is also represented in this figure by a bold green line.

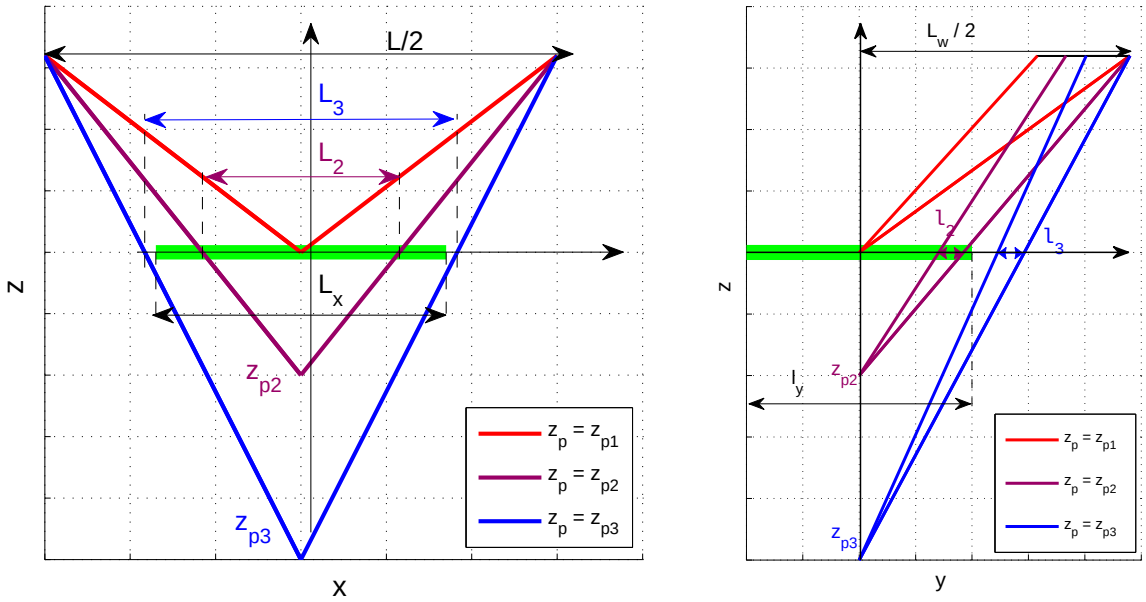

a) b)

Figure 6: The inverted pendulum during one step for three different pivot points.

We notice that the traveled distance by the CoP in **x** direction, increases when the pivot point depth increases ($L_2 < L_3$). Along the **y** direction, the CoP does not move when the pivot point is at ground level, but it moves in a range when the pivot point is under the ground. The range of the CoP along the **y** axis is increasingly far from the foot center when the $|z_p|$ increases. As we can see that l_2 is closer to the foot center than l_3.

For the bigger values of $|z_p|$, the CoP trajectory may leave the foot. For example, in Fig. 6, the CoP of the pendulum corresponding to z_{p3} leaves the contact zone between the foot and the ground. Therefore, for each foot size and step length and width, there is an upper limit of $|z_p|$ that keeps the CoP inside the foot.

For a robot with feet of length ℓ_x and width ℓ_y, performing a step of length L and width L_w, the upper limit of $|z_p|$ respects the following relation:

In the sagittal plane:

$$\frac{2\ell_x}{L} = \frac{|z_{p,max}|}{|z_{p,max}| + z_0} \qquad \text{if} \quad L > \ell_x \tag{13}$$

In the frontal plane:

$$\frac{\ell_y}{L_w} = \frac{|z_{p,max}|}{|z_{p,max}| + z_0} \qquad \text{if} \quad L_w > \ell_y \tag{14}$$

From these two equations, we can deduce the limit of z_p.

$$|z_{p,max,sagittal}| = \frac{2\ \ell_x\ z_0}{L - 2\ \ell_x} \qquad |z_{p,max,frontal}| = \frac{\ell_y\ \ z_0}{L_w - \ell_y} \tag{15}$$

The upper limit of $|z_p|$ is chosen as:

$$|z_{p,max}| = min(|z_{p,max,sagittal}|, |z_{p,max,frontal}|) \tag{16}$$

When we generate trajectories for experiments on a real robot, we should consider a security margin for CoP before calculating $|z_{\text{p,max}}|$. The security margin can be defined as a percentage of foot dimensions. In simulation, the security margin may be not considered.

The humanoid robot Romeo feet are 0.289 m in length and 0.121 m in width. By applying (16), we obtain: $|z_{\text{p,max}}| = 1.09\ m$. If we consider a margin of security of 50% of the foot, we obtain $|z_{\text{p,max}}| = 0.29\ m$. The robot foot with the security margin is illustrated in Fig. 7.

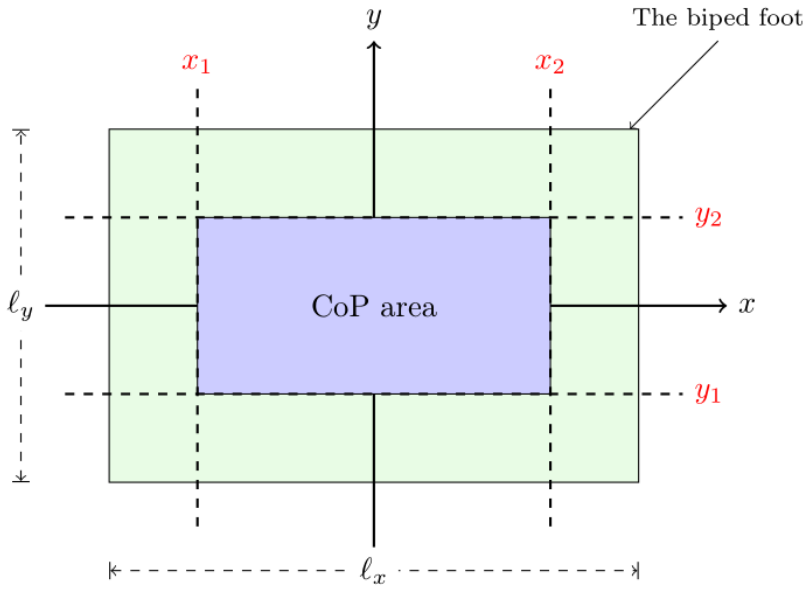

Figure 7: The foot and the CoP area.

6.3 Joint torque

In this section, we consider three trajectories for humanoid robot Romeo. One was calculated using an inverted pendulum with a pivot point at ground level (z_p=0). Another was calculated using an inverted pendulum with a pivot point under the ground ($z_p = -z_{\text{p,max}} = -0.29\ m$). A third one with a pivot point in the middle between $z_{\text{p,max}}$ and the ground, $z_p = -0.145\ m$).

The three inverted pendulums have the same parameters for step length, step width, step duration and CoM height as given in Sec. 5. We compare joint torques for these three trajectories.

Fig. 8 shows the torques at the legs joints. The support leg contains six joints: ankle roll (Γ_2), ankle pitch (Γ_3), knee pitch (Γ_4), hip pitch (Γ_5), hip roll (Γ_6), and hip yaw (Γ_7). The swing leg contains six joints also: ankle roll (Γ_{13}), ankle pitch (Γ_{12}), knee pitch (Γ_{11}), hip pitch (Γ_{10}), hip roll (Γ_9), and hip yaw (Γ_8).

In global, the three trajectories show similar behavior. We can see that Γ_5, Γ_{10}, Γ_{11}, and Γ_{12} are almost the same. For these joints, the torque is a little reduced (between 1.8% and 5.2%) with $z_p = -0.29\ m$ than with a pivot point at ground level.

For Γ_3, Γ_4, Γ_7, Γ_8, and Γ_9, we can observe two or three peaks for each torque. The torque amplitude peak-to-peak is reduced for $z_p = -z_{\text{p,max}}$ compared to the case $z_p = 0$ by 20%, 10.8%, 1.3%, 20.2% and 26% respectively.

The torque at the hip roll of the support leg Γ_6 is the only one that increases when the pivot point is under the ground level. The rate of increase when $z_p = -0.29\ m$ with respect to the case $z_p = 0$ is given at three times within the motion: 6.22% at ($t = 0sec$), 1.97% at (t=0.31sec) and 6.39% at ($t = 0.5sec$).

We can notice that main differences happen at ankle roll for the two legs, Γ_2 and Γ_{13}.

When the pivot point depth increases, Γ_2 decreases for small values of z_p. For example, $z_p = -0.145\ m$ leads to a high reduction rate of Γ_2 with respect to $z_p = 0$. We give the reduction rate at three moment within the motion: 87% at ($t = 0\ sec$), 61% at the peak ($t = 0.31\ sec$) and 86% at the end of the step ($t = 0.5\ sec$). After a certain value of the depth z_p, $|\Gamma_2|$ starts to increases. When $z_p = -0.29\ m$, Γ_2 is also

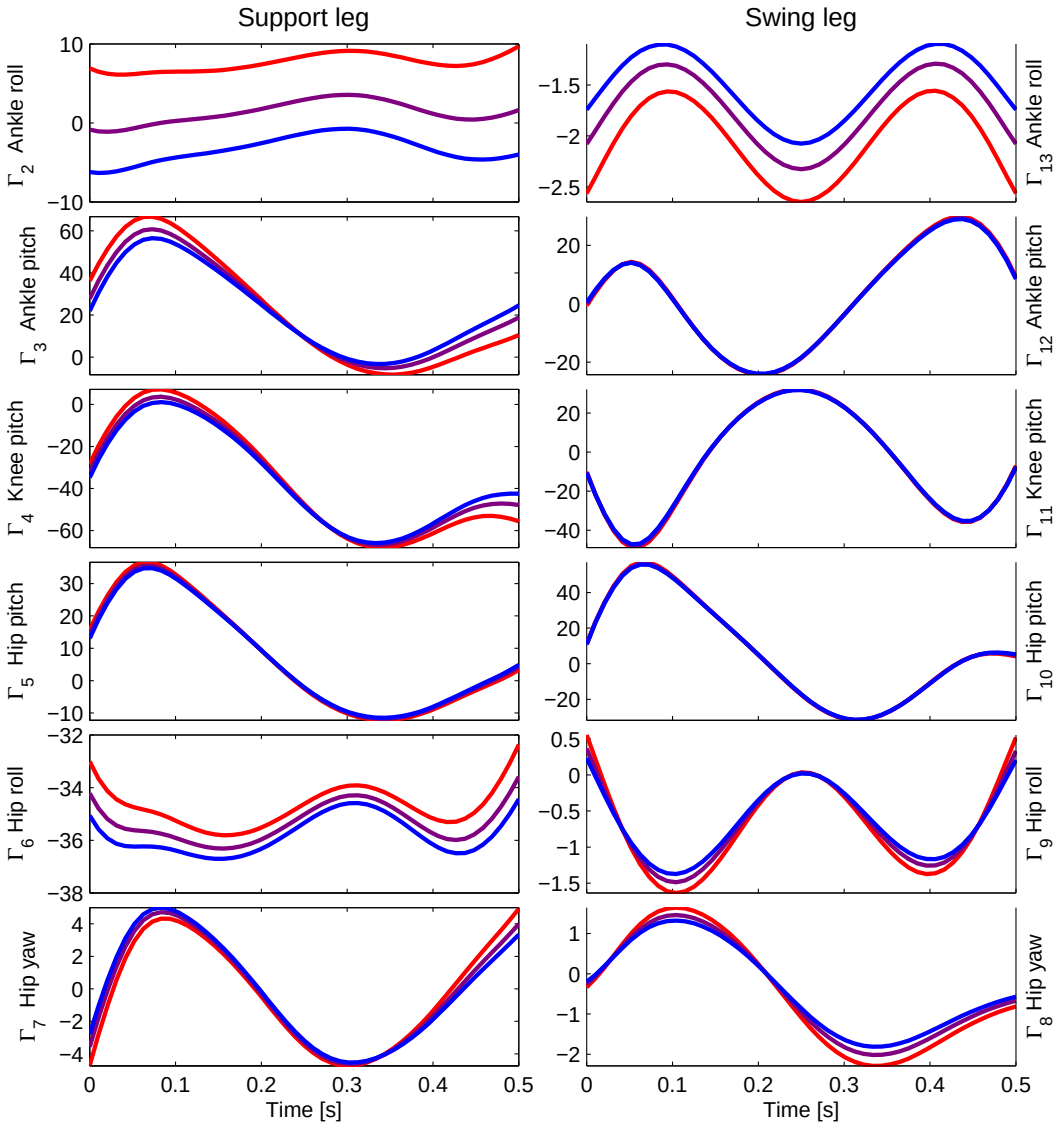

Figure 8: Joint torques for legs joints for 3 values of the pivot point depth (red curves for $z_p = 0$, purple curves for $z_p = -0.145\ m$ and blue curves for $z_p = -0.29\ m$).

reduced with respect to $z_p = 0$, but the reduction rate is smaller than in the case $z_p = -0.145\ m$. We give the reduction rate at three times within the motion: 9.8% at ($t = 0\ sec$), 91% at the peak ($t = 0.31\ sec$) and 58.8% at the end of the step ($t = 0.5\ sec$). When the pivot point is under the ground level, the pendulum rod gets longer, and the oscillation of the CoM along the lateral axis is reduced thereby (It can be seen in the left graph of Fig. 4). This reduction of the lateral oscillation of the CoM results in a reduction of joint variables for legs roll joint. For small depth of pivot point, the ankle-roll joint of the support leg, Γ_2, is relaxed. But for bigger values of z_p, the ankle-roll joint must support the body which does not oscillate widely in the lateral direction. So that, Γ_2 is overloaded in order to keep the equilibrium. This behavior may indicate an optimal value of the pivot point depth from the joint torques point of view.

The ankle roll of the swing leg, Γ_{13}, decreases when the pivot point depth increases. When $z_p = -0.29\ m$, Γ_{13} is reduced with respect to $z_p = 0$. We give the reduction rate at the three peaks: 29.4% at ($t = 0.1\ sec$), 21.6% at ($t = 0.25\ sec$) and 29.5% at ($t = 0.4\ sec$).

6.4 Energy evaluation

6.4.1 Sthenic criterion

The profile of the quadratic torque $E_0 = \Gamma^\top \Gamma$ during one step is shown in Fig. 9. The simulations were run with two values of the pivot point depth: $z_p = 0$ and $z_p = -0.29\ m$.

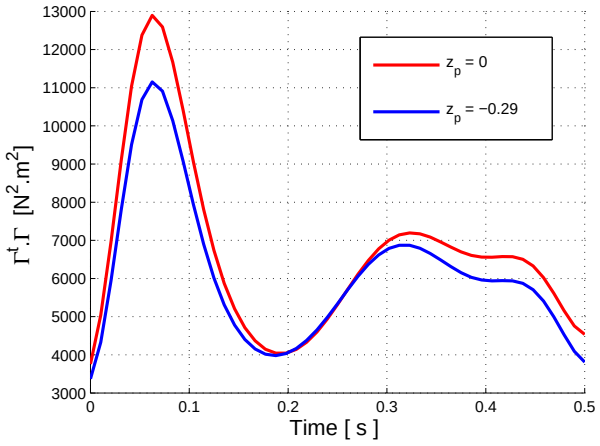

Figure 9: Quadratic torque

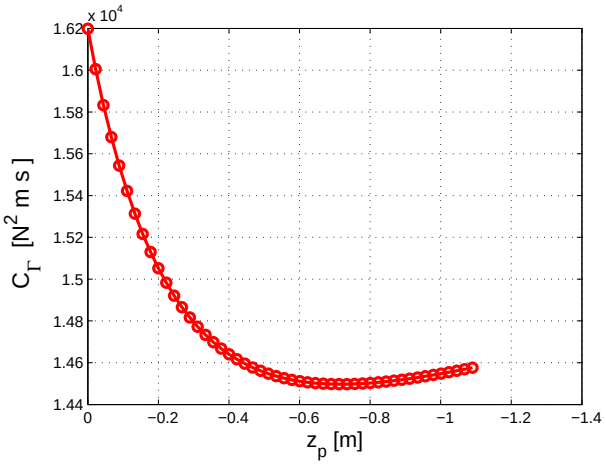

Figure 10: Sthenic criterion as a function of z_p.

Both graphs of Fig. 9 show a peak of value at the beginning of single supports followed by a valley at midstance. Fig. 9 shows that E_0 values at the beginning and at the end of the single support are lower with a pivot point under the ground level that with a pivot point at ground level. The evolution of the sthenic criterion as a function of the pivot point depth is shown in Fig. 10, for values of z_p between $[0\ -1.09]$ m, which is the maximum authorized in simulation. The situation $z_p = -0.718$ m minimizes the sthenic criterion, with the criterion value being reduced by 10.5% in comparison to the case $z_p = 0$. When we consider a security margin of 50% of foot dimensions, $z_{\mathrm{p,max}} = -0.29$ m corresponds to 9 % reduction of the sthenic criterion compared to the case $z_p = 0$.

6.4.2 Energy criterion

The energy consumption of the robot as a function of pivot point depth is also evaluated using the energy criterion C_E defined by equation (12). The energy criterion as a function of z_p is shown in Fig. 11. Energy

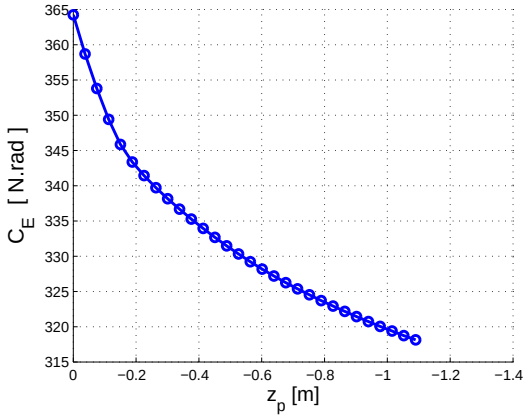

Figure 11: Energy criterion as a function of z_p.

criterion decreases as the depth of the pivot point increases. When $z_p = -1.09$ m, the energy criterion is reduced by 12.6 % compared to the case of a pivot point at ground level. When we consider a security margin of 50% of foot dimensions, $z_{\mathrm{p,max}} = -0.29$ m corresponds to 7 % reduction of the energy criterion compared to the case $z_p = 0$.

Contrary to the sthenic criterion, the energy criterion does not have a local minimum, but it decreases monotonically as the pivot point depth increases.

6.4.3 Step length consideration

The purpose of this section is to analyze the behavior of the system in other parameters sets. In other words, we want to show that reducing the sthenic criterion for deeper pivot points, that we obtained for a set of operating parameters, is not a special case. For this, we consider six values of step length, taken in the interval [0.2 0.4] m. For each step length, we examine the behavior of the sthenic and the energy criteria as a function of the pivot point depth.

Fig. 12 shows the evolution of the sthenic criterion for each considered step length. The overall behavior

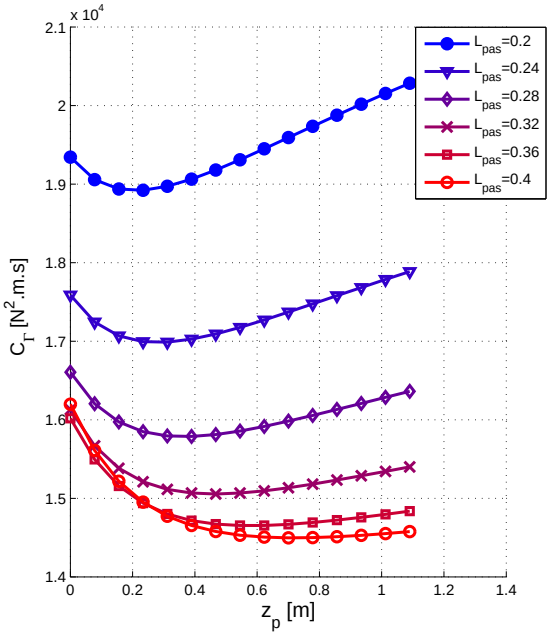

Figure 12: Sthenic criterion as a function of step size.

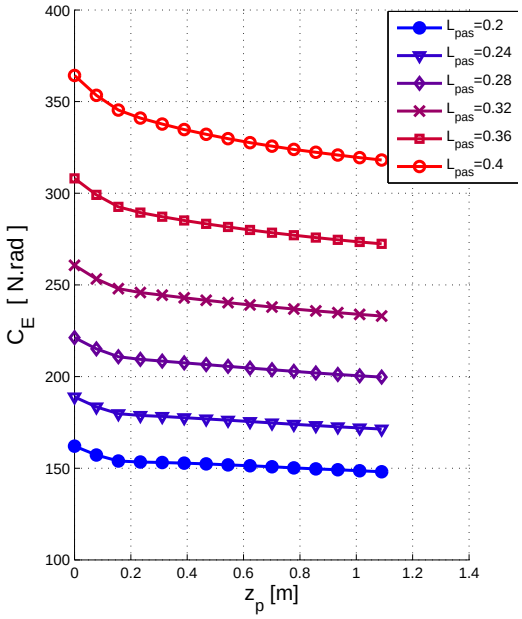

Figure 13: Energy criterion as a function of step size.

is the same for all step lengths. The sthenic criterion decreases as the depth of the pivot point increases, it reaches a local minimum at certain value of z_p, then it starts to increase.

For longer steps, the maximal reduction rate of sthenic criterion when z_p increases, is more important. This rate is 10 %, 6 %, and 1 % for $L = 0.4$ m; 0.32 m; and 0.2 m respectively. Moreover, one can observe that the z_p value that minimizes sthenic criterion is smaller for smaller steps. We also notice that the sthenic criterion is lower for the longest step of the same duration.

These findings concern the role of the step length without changing the step time, and may change in the case where the step duration is adapted to the step length.

Fig. 13 shows the evolution of the energy criterion as a function of the pivot point depth for each considered step length. The overall behavior of the energy criterion is similar for the six studied step lengths: It decreases monotonically as the depth of the pivot point increases.

For longer steps, the reduction rate of the energy criterion when z_p increases, is more important. This rate is 12.6 %, 10.6 %, and 8.6 % for $L = 0.4$ m; 0.32 m; and 0.2 m respectively. We also notice that the energy criterion is lower for the smallest step of the same duration. This is due to the definition of the energy criterion which is proportional to the velocity.

7 Conclusion

This paper proposed an analysis of the effect of the vertical position of the pivot point on the energy consumption for humanoid walking gait. A 3D simulation was carried out to compare the classical inverted pendulum with a pivot point on the ground level and an inverted pendulums with a pivot point under the ground level. The dynamics analysis showed that the use of a pivot point under the ground reduced reasonably the joint torques, especially in the beginning of the single support. Moreover, the sthenic criterion can be

minimized for an optimal pivot point depth. The results can be included in walking pattern generators in order to reduce energy consumption during walking.

In addition, the presented method allows the CoP to travel along the supporting foot. The advancement of the CoP from the heel to the foot tip, allows the robot to move the contact zone between the foot and the ground within the single support to follow the CoP. In other words, this human-like trajectory of CoP can be used in the future for the generation of rolling of feet.

References

[Kaj91] S. Kajita, and K. Tani, Study of dynamic walk control of a biped robot on rugged terrain - Derivation and application of the linear inverted pendulum mode. In Transactions of the Society of Instrument and Control Engineers. 27:177–184, 1991.

[Che01] Ch. Chevallereau and Y. Aoustin. Optimal reference trajectories for walking and running of a biped robot. In Robotica, 19:557–569, 2001.

[Che08] Ch. Chevallereau, G. Bessonnet, G. Abba, and Y. Aoustin, Bipedal Robots. Wiley, 2008

[Kaj01] S. Kajita, F. Kanehiro, K. Kaneko, K. Yokoi, H. Hirukawa. The 3D Linear Inverted Pendulum mode: A simple modelling biped walking pattern generation. In Proceedings of the 2001 IEEE/RSJ International Conference on Intelligent Robots and Systems, Maui, Hawaii, USA 2001.

[Omr14] S. Omran, S. Sakka, Y. Aoustin. Effects of the vertical CoM motion on energy consumption for walking humanoids. In Proceedings of the 17th International Conference on Climbing and Walking Robots and the Support Technologies for Mobile Machines, 2014.

[Sak10] S. Sakka, Ch. Hayot, P. Lacouture. A generalized 3D inverted pendulum model to represent human normal walking. In IEEE-RAS International Conference on Humanoid Robots, 2010.

[Ald12] Robotics Aldebaran. Romeo humanoid robot documentation, 2012.

[Ais98] AIST. HRP-2. http://global.kawada.jp/mechatronics/hrp2.html since 1998

[Har09] K. Harada, K. Miura, M. Morisawa, K. Kaneko, SH. Nakaoka, F. Kanehiro, T. Tsuji, and S. Kajita. Toward human-like walking pattern generator. In The 2009 IEEE/RSJ International Conference on Intelligent Robots and Systems, 2009.

[Hon96] Honda Motor Co. ASIMO. http://world.honda.com/ASIMO/ since 1996

[UT01] The University of Tokyo. UT-Theta. http://www.ynl.t.u-tokyo.ac.jp/research/ut_theta/ since 2001

[Haq12] A. Haq. Strategies for energy storage during a walking step of a bipedal robot. PHD thesis, Université de Nantes, 2012.

[Ber08] B. Berret, and C. Darlot, and F. Jean, and T. Pozzo, and C. Papaxanthis, and J. Gauthier. The inactivation principle: mathematical solutions minimizing the absolute work and biological implications for the planning of arm movements. In PLoS Computational Biology, 4(10) doi: 10.1371, 2008.

[Ack12] E. Ackerman. Aldebaran Robotics Introduces Romeo, Finally. In IEEE Spectrum, 2012.

[Hay13] C. Hayot, and S. Sakka, and V. Fohanno, and P. Lacouture. Biomechanical modeling of the 3D center of mass trajectory during walking. In Movement and Sport Sciences - Science and Motricité, 2013.

[Soe95] J. F. Soechting, and Ch. A. Bunco, and U. Herrmann, and M. Flanders. Moving Effortlessly in Three Apply to Arm Movement. In The Journal of Neuroscience, 15(9) 6271–6280, 1995.

[Zij97] W. Zijlstra and At L. Hof. Displacement of the pelvis during human walking : experimental data and model predictions. In Gait & Posture, 6(3) 249–262, 1997.